ARTICLE

Check for updates

Biomarkers in the rock outcrop of the Kazusa Group reveal palaeoenvironments of the Kuroshio region

Hiroto Kajita [1,2,3,4✉], Ayumi Maeda[1,2,3,4], Masayuki Utsunomiya[3], Toshihiro Yoshimura [4],
Naohiko Ohkouchi[4], Atsushi Suzuki[3] & Hodaka Kawahata[1,2]

Long-chain alkenones and *n*-alkanes preserved in marine and lake sediment cores are widely used to reconstruct palaeoenvironments. However, applying this technique to exposed sedimentary rock sequences is relatively challenging due to the potential for the diagenetic alteration of organic biomarkers. Here, we extract long-chain alkenones and *n*-alkanes from an exposed outcrop of the Kazusa Group in central Japan, one of the most continuous sedimentary successions in the world, covering almost the entire Pleistocene. We find that the alkenone unsaturation ratio and average chain length of *n*-alkanes appears to reflect the glacial-interglacial changes in sea surface temperature and terrestrial climate, respectively. Alkenone-based sea surface temperatures between 1.1 and 1.0 million years ago concur with foraminiferal Mg/Ca-based temperature estimates and may reflect an intrusion of the Kuroshio Current. We suggest that the preservation of these biomarkers in the Kazusa Group demonstrates its potential to provide a detailed palaeoenvironmental record.

[1] Atmosphere and Ocean Research Institute, The University of Tokyo, Kashiwa, Japan. [2] Department of Earth and Planetary Science, Graduate School of Science, The University of Tokyo, Tokyo, Japan. [3] Geological Survey of Japan, National Institute of Advanced Industrial Science and Technology, Tsukuba, Japan. [4] Biogeochemistry Research Center, Japan Agency for Marine-Earth Science and Technology, Yokosuka, Japan. ✉email: kajita322@frontier.hokudai.ac.jp

ong-chain alkenones (LCAs) are C_{35}–C_{42} unsaturated methyl and ethyl ketones with 2–4 double bonds and feature unique lipid biomarkers produced by Isochrysidales hapto-phytes living in surface waters[1]. The degree of unsaturation in C_{37} alkenones ($U^{K'}_{37}$) is strongly correlated with the growth temperature in culture experiments and is widely used as one of the most quantitative and well-established proxies for sea surface temperature (SST)[2–4]. High-molecular (>C_{27}) n-alkanes with odd/even predominance are derived from terrestrial higher plants[5,6] and are used to reconstruct changes in the temperature, humidity, and vegetation based on the carbon number distributions[7,8]. These palaeoenvironmental indices are traditionally applied to marine and lake sediment cores, but are rarely applied to exposed sedimentary rocks because LCAs and n-alkanes can undergo maturation at high temperature and lose their initial palaeoenvironmental information[9,10]. Several previous studies have detected LCAs and n-alkanes from outcrops; however, only a few studies conducted on the outcrops around the Mediterranean Sea, have successfully discussed high time-resolution (glacial-inter-glacial-scale) climate changes using $U^{K'}_{37}$, and there are no studies in which n-alkane-based indices have been used[7,11,12].

The Kazusa Group represents the infill of the Plio-Pleistocene Kazusa forearc basin that developed in response to the subduction of the Pacific and Philippine Sea plates beneath the North American plate, and is well exposed in the Boso Peninsula, Chiba Prefecture, central Japan[13] (Fig. 1). The middle to lower part of the Kazusa Group is represented by successions of submarine fan deposits associated with deep-sea, basin-plain, and slope deposits accumulated during the Pleistocene, which is characterised by continuous and well exposed sedimentary successions with a high sedimentation rate (ca. 1.5 m kyr^{-1} on average)[13,14]. It contains marine microfossils, palaeomagnetic reversals, and a large number of tephra beds, which allow us to establish a robust chronological and stratigraphic framework and undertake palaeoceanographic and palaeoclimatic studies with high time-resolution[15–19] (Fig. 2). These studies are recognised worldwide, and the Chiba composite section in the Kazusa Group was ratified in 2020 as the Global Boundary Stratotype Section and Point (GSSP) to define the boundary of the Chibanian and Calabrian stages[20].

The Boso Peninsula is located near the Kuroshio Extension Front (KEF), where the Kuroshio Current (KC) leaves the coast of Japan. The KC transports warm and saline water from the equatorial Western Pacific Warm Pool (WPWP) to northern mid-latitudes, and forms pronounced latitudinal gradients in SST

off the Boso Peninsula[21] (Supplementary Fig. 1). It is also located at the northern limit of the seasonal progression of the westerly jet that bounds the East Asian monsoon (EAM) front[22]. Thus, the oceanic and terrestrial conditions around the Kazusa forearc basin should be responsive to shifts in the KEF and EAM, which are related to the modulations in the dynamics of Hadley cells in the northern hemisphere[21,22]. Therefore, the palaeoenvironmental information, especially SST, stored in the Kazusa Group could be important for understanding the changes in global climate systems during the Pleistocene. However, there has been no widely applicable quantitative proxy for SST owing to the extremely small standing stock and poor preservation of surface-dwelling planktic foraminifera. In this study, we discovered that multiple classical biomarkers, LCAs and odd preference n-alkanes, are well preserved in several sections of the Kazusa Group and can be used as palaeoenvironmental indicators.

Geological setting and sample collections. The Otadai Formation in the Kazusa Group consists of alternations of turbidite sandstone and hemipelagic siltstone beds which had developed as deep-sea submarine fan systems from 1.2 to 1.0 Ma[13]. Frequently intercalated tephra beds in the Otadai Formation allow lateral bed-by-bed correlation of turbidite sandstone and siltstone beds[23]. Detailed oxygen isotope stratigraphy for the upper to middle Otadai Formation was established using benthic foraminifera recovered from the TR-3 core, which was confirmed by fission-track ages of zircon from key intercalated tephra beds, as well as magnetostratigraphy and biostratigraphy[24]. This chronological model was applied by correlations between TR-3 and the outcrops using comparison with key tephra beds (named O4, O4.5, O7, O11, O12, O16 and O18)[24], which were identified based on visual observations, mineral compositions, and refractive index of volcanic glass[24]. We collected samples from the middle part of the Otadai Formation, corresponding to Marine Isotope Stage (MIS) 33–29, exposed along the Yoro River (Yoro River route in Supplementary Fig. 2a) and a creek running through the Shoryuji district (Shoryuji route in Supplementary Fig. 2b) located ca. 10 km east of the Yoro River route (Fig. 3). A visibly weathered surface coating (2–65 cm in depth) is commonly seen in the outcrops of the Kazusa Group, where oxidation causes dissolution of pyrite, a decrease in organic matter, and increase in ferric oxide[25] (Supplementary Fig. 3). All samples, except the samples S-29-7 (brownish-red weathered sample),
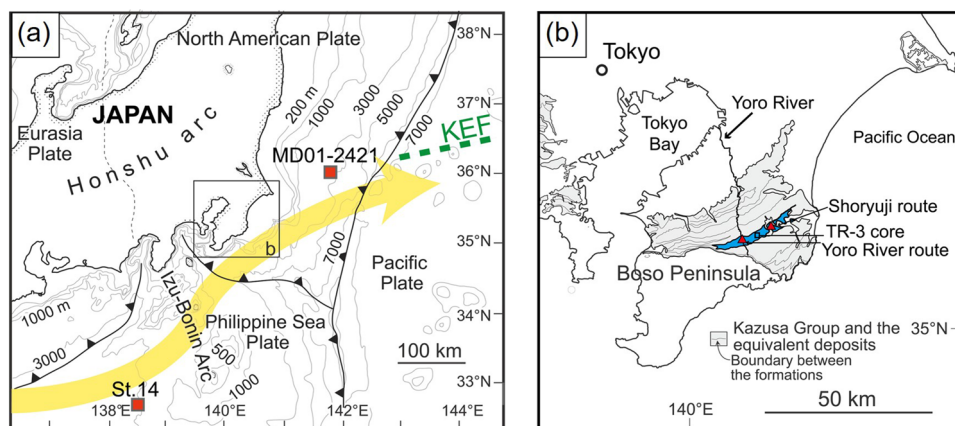
Fig. 1 Maps showing the overall setting of the Kazusa Group in central Japan. a Bold yellow arrow and green dotted line represent the general path of the KC and KEF in the present day, respectively. The bathymetry, plate boundaries, and locations of cores MD01-2421 and St. 14 (red squares) are also shown. **b** Surface distribution of the Otadai Formation (blue-coloured) in the Kazusa Group (grey-coloured) on the Boso Peninsula[26,27], showing the locations of the survey sites in this study (red triangles) and the TR-3 core (open square). The figures were generated using Generic Mapping Tools[58].
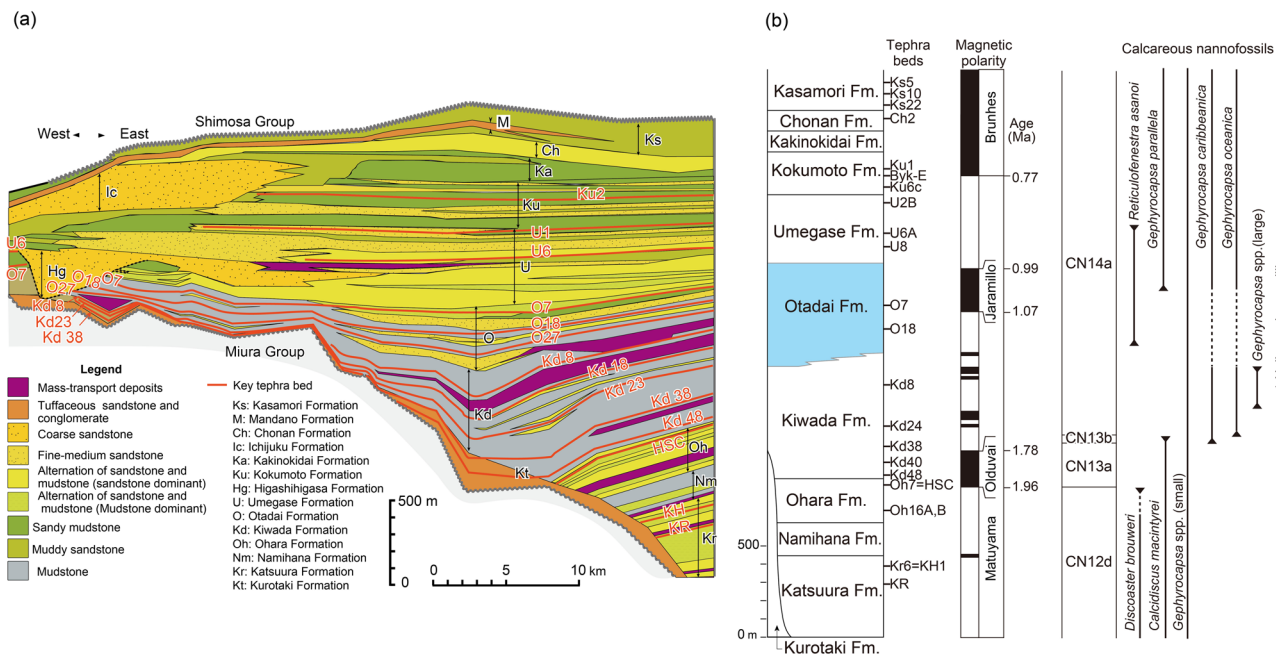
Fig. 2 Geotectonic background of the Pleistocene Kazusa Group on the Boso Peninsula, central Japan, summarised in Utsunomiya et al.[59].
a Stratigraphic east-west cross-section and **b** chronostratigraphy of the Kazusa Group on the Boso Peninsula.

were taken from the fresh part in bluish-grey colour exposed after removing the brownish-red surface coating. To investigate the spatial data variability, six samples (S-29-1–6) were taken from the siltstone bed along the depositional plane, ca. 10 cm below the O18 key tephra bed exposed along the Yoro River route (Fig. 4). In addition, a brownish-red weathered sample (S-29-7) from the same location as sample S-29-6 and a turbidite sandstone sample (S-29-8) from directly beneath sample S-29-6 were taken (Fig. 4). The O7 and O11 key tephra beds were also exposed along the Shoryuji route[26,27]. Siltstone samples were taken directly above and below the O7 and O11 key tephra beds on each route to compare data obtained from the same stratigraphic level (Fig. 3).

Results and discussion
LCAs and _n_-alkane-based proxies as palaeoenvironmental indices. C_{37}–C_{39} LCAs and odd preference C_{26}–C_{36} _n_-alkanes were detected in all samples analysed in this study (Fig. 5; all data are available in Supplementary Data 1). The excellent preservation of these biomarkers is probably because the Kazusa Group has never suffered from high temperatures or consolidation stress during burial and uplift. The palaeo-maximum temperature and maximum burial depth deduced from vitrinite reflectance and consolidation tests in the Otadai Formation were <45 °C and 7.6 MPa, respectively[28]. According to hydrous pyrolysis experiments, the LCAs and _n_-alkane-based indices do not change under these conditions at laboratory time scales (~days)[9,10]. The weakly consolidated soft rock is susceptible to physical erosion; therefore, fresh material that has not been chemically weathered is exposed on the riverside, which is advantageous for biomarker preservation.

The alkenone unsaturation ratio ($U_{37}^{K'}$), average chain length (ACL) and carbon preference index (CPI) of _n_-alkanes were defined as follows:

$$U_{37}^{K'}(=\{C_{37:2}\}/\{C_{37:2}\} + \{C_{37:3}\}),$$

$$ACL(=x[C_x]/[C_x]),$$

$$CPI(=2\times[C_x]/([C_y]+[C_z])),$$

where { } and [ ] represent the concentrations of each carbon number of LCAs and _n_-alkanes, respectively ($x = 27, 29, 31, 33, 35$; $y = 26, 28, 30, 32, 34$; $z = 28, 30, 32, 34, 36$).

The spatial data variabilities (1σ) of $U_{37}^{K'}$, ACL and CPI in the single siltstone bed just below the O18 key tephra bed were 0.008, 0.123 and 0.434, respectively, which were significantly small compared to the overall range of variations (Table 1). The ACL and CPI values of the weathered surface coating were the same as those of the fresh siltstone, whereas $U_{37}^{K'}$ showed higher values for the former (Table 1). This might be due to the preferential decrease of triunsaturated C_{37} alkenones ($C_{37:3}$) compared to diunsaturated C_{37} alkenones ($C_{37:2}$) under long exposure to oxidative conditions[9]. Therefore, removing weathered coatings is important to obtain the initial $U_{37}^{K'}$ values, as was also shown in another study on the outcrop[11]. The turbidite sand bed, which might have been redeposited from a shallower seabed[23], had a significantly lower CPI value than the siltstones (Table 1). CPI may be decreased through dilution and degradation of terrestrial plant-derived material during the redeposition process because _n_-alkanes derived from bacteria and algae have even carbon numbers[5,6]. In contrast, the turbidite sandstone and adjacent siltstones had similar $U_{37}^{K'}$ and ACL values (Table 1), which indicates that these values changed negligibly in the redeposition process, as is also suggested by Prahl and co-workers[29]. The $U_{37}^{K'}$, ACL and CPI values of the siltstone beds of the Shoryuji route coincided with the values from the correlative beds of the Yoro River route within the data variability (1σ) of the single siltstone bed, which confirms that these indices are immune to the effects of topography of the submarine fan and faithfully reflect the representative environment around the Kazusa forearc basin (Fig. 6).

$U_{37}^{K'}$, ACL and CPI of the Yoro River route samples ranged between 0.795–0.921, 30.1–31.0 and 3.66–6.02, respectively, showing variations synchronised with the glacial and interglacial cycles from MIS 33 to 29 (Fig. 7). However, the relative compounds of total organic carbon and total nitrogen (C/N ratios), indicating relative contributions of terrestrial and marine organic matter (see 'Methods' for details), were not completely
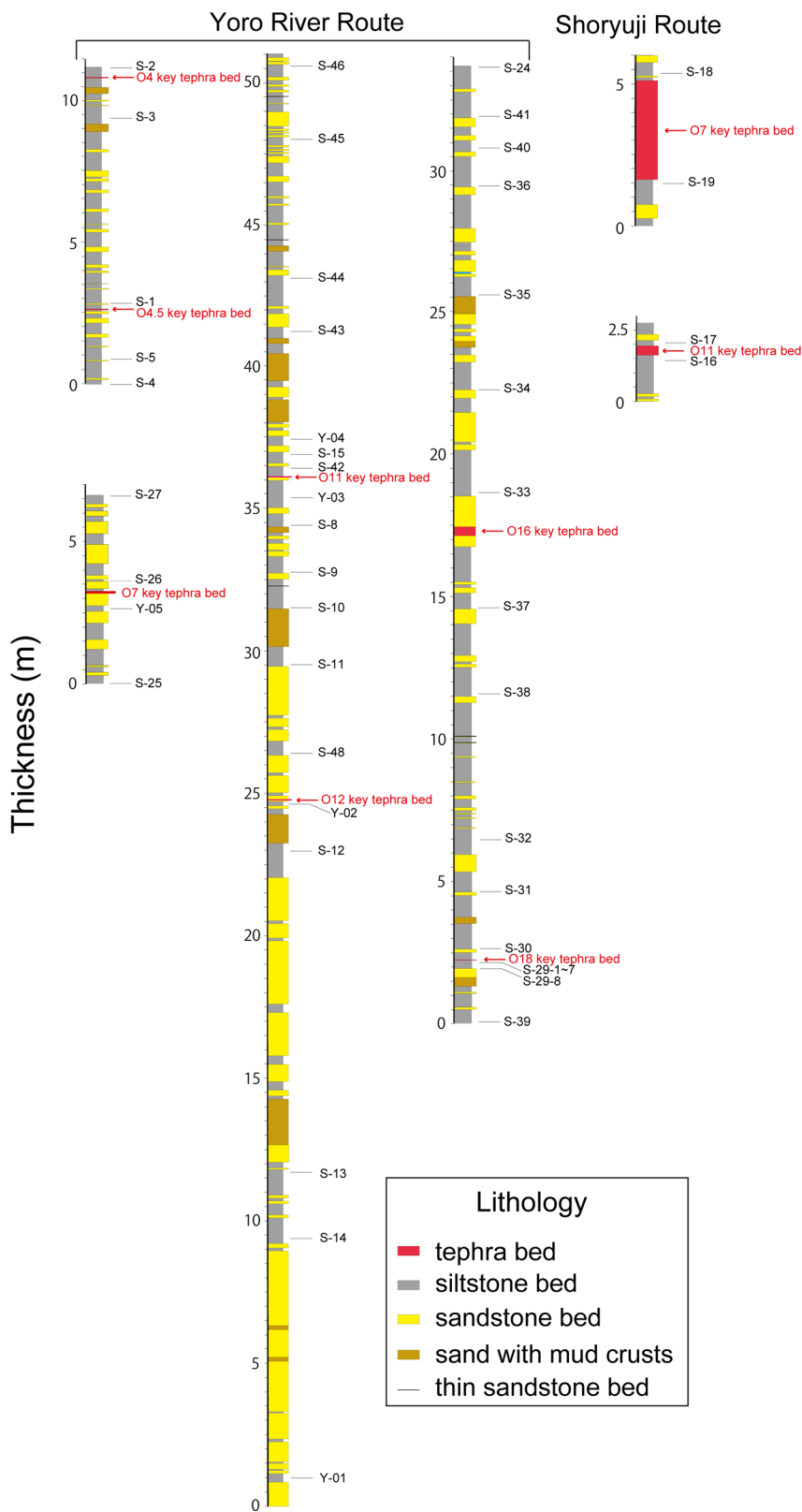
Fig. 3 Simplified lithology of the Otadai Formation considered for this study. The figure shows the sampling horizons along the Yoro River and Shoryuji routes with the intercalated key tephra beds.

synchronised with the glacial-interglacial cycles, suggesting that the accumulation process of organic compounds was controlled not only by sea-level changes but also by the effects of topography and redeposition in submarine fans (Fig. 7). $U_{37}^{K'}$ must reflect the temperature fluctuation in the Kazusa forearc basin at water depths of 0–50 m, where LCAs are mostly produced[30]. The transportation routes of n-alkanes are enigmatic because they can be supplied not only as river suspensions but also as aeolian dust[31]. However, we believe that ACL and CPI fluctuations mostly reflect monsoonal climate changes in the hinterland of the
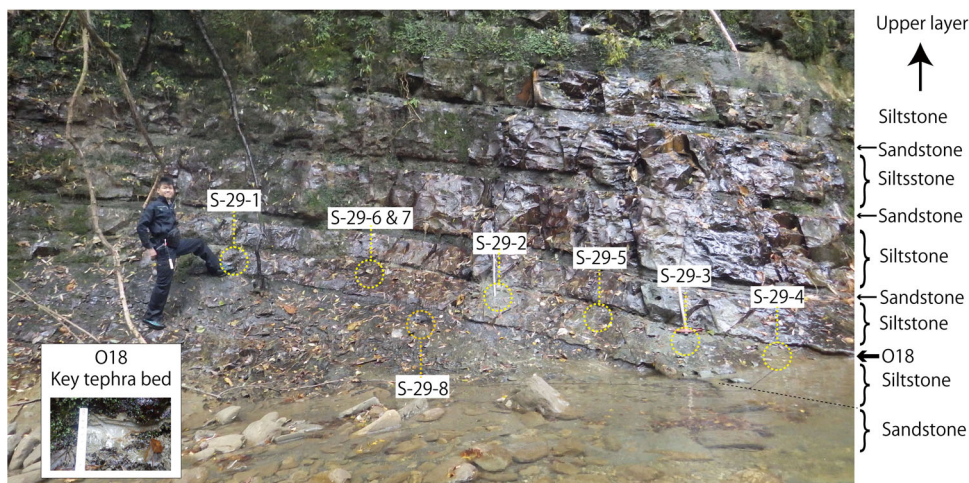
Fig. 4 Locations of the sampling points for estimating spatial data variability. The photograph shows the sampling points (demarcated in yellow circles) in the siltstone and sandstone beds below the O18 key tephra bed.
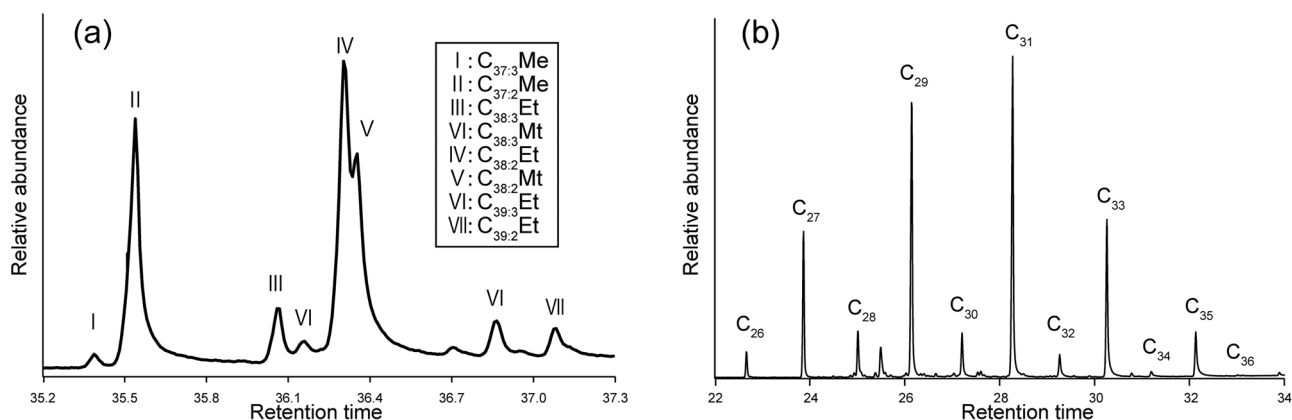
Fig. 5 GC-MS analysis results. Representative GC-MS chromatograms of **a** LCAs and **b** n-alkanes in sample S-8 taken from between the O11 and O12 key tephra beds.

Table 1 Spatial variations of multiple proxy records along the depositional plane within the siltstone bed just below the O18 key tephra bed (Samples S-29-1 to S-29-6).

Sample ID	$U_{37}^{K'}$	$U_{37}^{K'}$-SST (°C)	ACL	CPI	C/N
S-29-1	0.912	26.3	30.6	4.91	7.7
S-29-2	0.893	25.7	30.4	5.09	8.1
S-29-3	0.912	26.3	30.4	4.89	8.4
S-29-4	0.911	26.3	30.7	4.72	9.3
S-29-5	0.898	25.9	30.5	3.96	9.4
S-29-6	0.899	25.9	30.6	4.27	8.4
Average	0.904	26.1	30.6	4.64	8.6
1σ	0.008	0.254	0.123	0.434	0.690
S-29-7	0.943	27.2	30.4	4.96	11.0
S-29-8	0.916	26.4	30.8	2.36	11.7

The values from the surface weathered material (S-29-7) and the turbidite sandstone bed (S-29-8) just below the siltstone bed are also shown. The detailed sampling location horizons are shown in Fig. 4.

Kazusa forearc basin because higher ACL and lower CPI values have been detected in the lower latitudes for the present-day surface soils in East Asia as well as for the aerosols of the western Pacific[32–34]. CPI values are weakly correlated with C/N ratios

($R^2 = 0.31$, $p < 0.01$) (Fig. 8), which indicates that they are also influenced by the freshness of n-alkanes controlled by the offshore transportation process[35]. $U_{37}^{K'}$ and ACL are not correlated with C/N ratios (Fig. 8); therefore, we conclude that these proxies are less susceptible to the effects of the sedimentation process and diagenesis, and can be excellent palaeoenvironmental indicators for the Kazusa forearc basin. The periods and amplitudes of the terrestrial climate fluctuations indicated by ACL were almost synchronised with those of the oxygen isotope ratios of benthic foraminifera ($\delta^{18}O_{BF}$) (Fig. 7a, c). $U_{37}^{K'}$ values in the moderate interglacial periods (MIS 29 and 33) were comparable with those in the extreme interglacial period (MIS 31) (Fig. 7a, b). The reason for the difference in the fluctuation pattern of $U_{37}^{K'}$ and those of ACL and $\delta^{18}O_{BF}$ can be attributed to the effect of ocean currents, as discussed in the next section.

Quantitative temperature reconstructions and implications for palaeoceanography. We calculated the $U_{37}^{K'}$-SST using the global core-top calibration[3], which is largely consistent with the culture calibration of the modern alkenone synthesiser[2]. The temperature calibration may be affected by changes in the assemblages of the alkenone synthesisers, but the evolutionary events and changes in species dominance within the coccolithophore populations are considered to have had little impact on the relationship between $U_{37}^{K'}$ and SST during the Pleistocene[36,37]. The $U_{37}^{K'}$-SSTs during
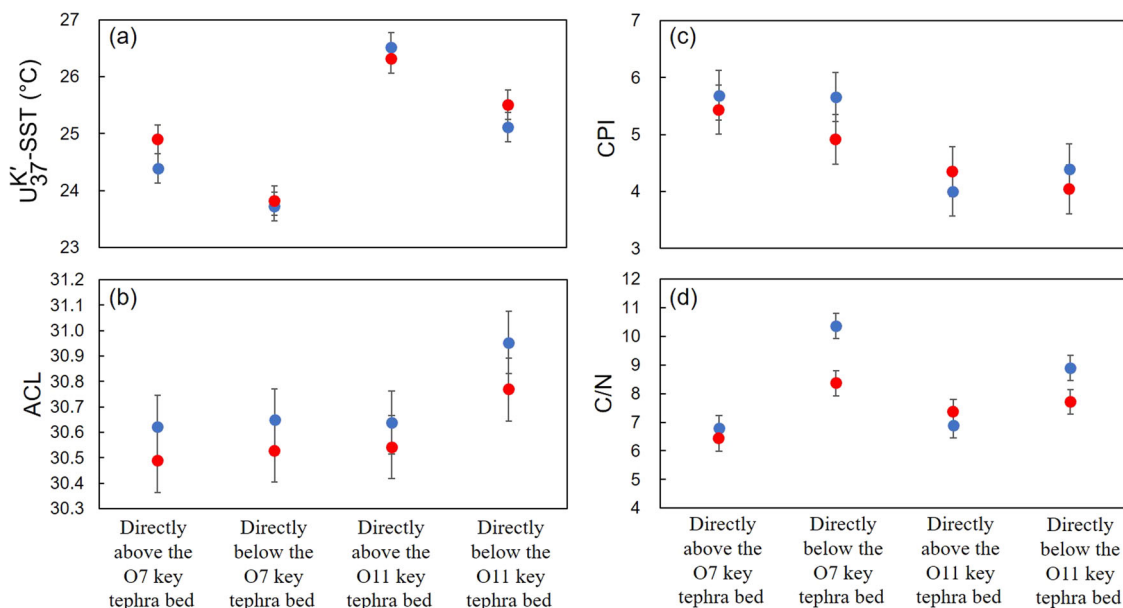
Fig. 6 Comparison of biomarker-based indices and C/N ratio in the strata of the Yoro River and Shoryuji routes. Blue and red circles represent the indices **a** $U_{37}^{K'}$-SST, **b** ACL, **c** CPI and **d** C/N ratio, at the same level of the Yoro River and Shoryuji routes, respectively. The error bars indicate the standard deviations based on six samples taken from the siltstone bed (S-29-1–6) (Table 1).
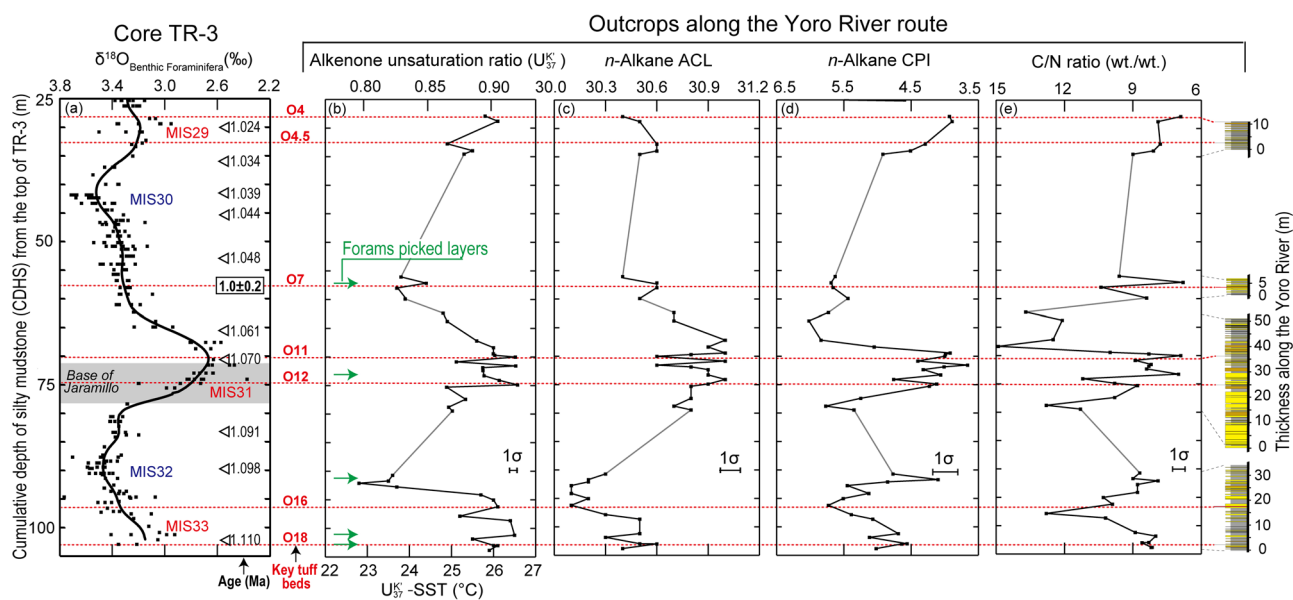
Fig. 7 Results of biomarker-based indices and C/N ratio along the Yoro River route. a Oxygen isotope stratigraphy of the TR-3 core, which is comparable to the Yoro River route[24]. Triangles show age-control horizons established by correlation with deep-sea core ODP site 677. The base of the Jaramillo normal subchronozone is shown with the shaded area. The intercalated key tephra beds are shown with dotted lines, one of which (O7) was dated by zircon fission track (1.0 ± 0.2 Ma). **b** $U_{37}^{K'}$, **c** ACL, **d** CPI and **e** C/N ratios of the outcrops along the Yoro River route. Grey lines connect the strata from which samples for biomarker analysis were not collected because of the far distance from the key tephra beds. The error bars indicate the standard deviations based on six samples taken from the siltstone bed (S-29-1–6) (Table 1).

MIS 33 to 29 were calculated from 22.8 to 26.6 °C. Fluctuations in the $U_{37}^{K'}$-SST near the Boso Peninsula have been previously reported from the core site of MD01-2421 covering MIS 1–5e[38] (Fig. 1). Comparing periods with similar ice volumes estimated from the global $\delta^{18}O_{BF}$ profile[39,40], the $U_{37}^{K'}$-SSTs in the Otadai Formation appeared to be 4–7 °C higher than those of the MD01-2421 core, located near the KEF (Table 2). The ratio of magnesium to calcium (Mg/Ca) of planktic foraminifera is an additional established palaeotemperature proxy[41]. From the five selected

beds with relatively large amounts of foraminiferal standing stock, we analysed Mg/Ca palaeotemperatures of *Globigerina bulloides* (T_{bul}), which were abundant at depths shallower than 40 m near the Boso Peninsula[42]. T_{bul} showed 19.9–21.9 °C and 22.5–24.8 °C in the glacial and interglacial periods, respectively, and these values are at least 4 °C higher than the T_{bul} from the MD01-2421 core[43], thereby supporting the validity of the high $U_{37}^{K'}$-SST (Table 2). The 1–4 °C offsets between the $U_{37}^{K'}$-SST and T_{bul} can be attributed to differences in the production seasons near the Boso
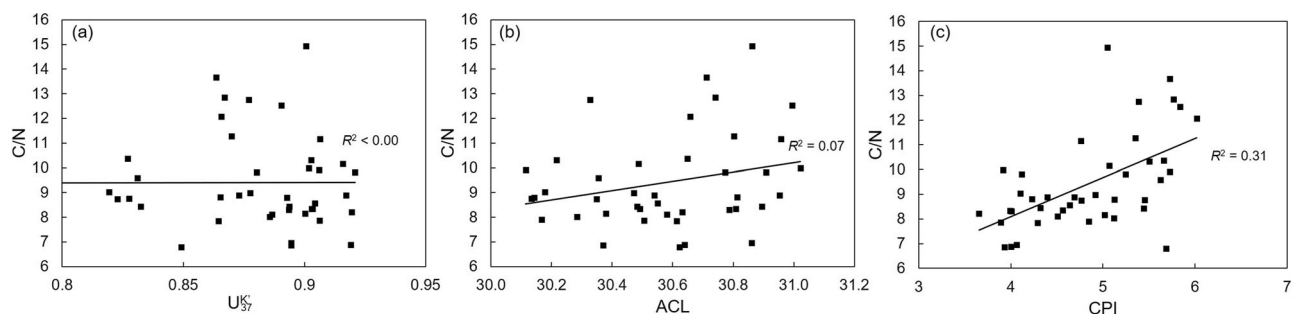
Fig. 8 Correlations between the C/N ratio and biomarker-based indices. a $U^{K'}_{37}$ and C/N ratio, **b** ACL and C/N ratio and **c** CPI and C/N ratio. The coefficient of determination (R^2) is also shown.

Table 2 Palaeotemperatures estimated from $U^{K'}_{37}$ and Mg/Ca ratios of _Globigerina bulloides_ in the Otadai Formation.

Location	Sample ID	MIS	$U^{K'}_{37}$-SST (°C)	Mg/Ca-SST (°C)
Otadai F.	S-29	33	26.1	23.3
Otadai F.	S-32	33	26.5	22.5
Otadai F.	S-24	32	23.6	21.9
Otadai F.	S-10	31	25.7	24.8
Otadai F.	S-26	30	24.3	19.9
MD01-2421		5e	ca. 20–23	–
MD01-2421		5a-d	ca. 19–21	–
MD01-2421		4	ca. 18	–
MD01-2421		3	ca. 17–19	–
MD01-2421		2	ca. 13–16	ca. 7–8
MD01-2421		1	ca. 17–21	ca. 16–18
St.14		2	ca. 20–22	–
St.14		1	ca. 22–24	–

Data from core MD01-2421[38,43] and St. 14[48] are also shown.

Peninsula, insofar as LCAs are mostly produced in July[30], whereas _G. bulloides_ are most abundant during the spring phytoplankton bloom[44]. Although these temperature offsets do not seem to be constant, similar trends have often been reported in previous studies conducted on marine sedimentary cores[45,46]; this is because the high production season for _G. bulloides_ can differ, as their production is greatly influenced by nutrient availability[47].

To better understand the environment of the Kazusa forearc basin, we compared our data with the $U^{K'}_{37}$ data reported for sediment cores surrounding the Boso Peninsula. The $U^{K'}_{37}$-SSTs in the Otadai Formation were still 2–3 °C higher than those reported from the St. 14 core covering MIS 1–2, located near the mainstream of the KC[48] (Fig. 1, Table 2). Considering the distribution of SSTs around the core sites of MD01-2421 and St. 14 (Supplementary Fig. 1), we interpret that the Kazusa forearc basin was located under the direct influence of the KC, and the temperatures of the warm water masses in the interglacial periods (MIS 29, 31 and 33) may have been higher than those in the Holocene (MIS 1). We also assumed that the KC could still have had a large influence on the Kazusa forearc basin even in the glacial periods (MIS 30 and 32) compared to those in the last glacial period (MIS 2) when the KEF had shifted to the south[48,49]. Previous studies using marine sediment cores have revealed 1–2 °C higher SSTs in the California margin and eastern equatorial Pacific from 1.1 to 1.0 Ma compared to the present day, while SSTs in the western equatorial Pacific have remained nearly the same[50,51]. Our study, the documentation of quantitative SSTs recorded near the KEF, revealed that the latitudinal temperature gradient in the north-western Pacific was small, indicating the widespread WPWP from 1.1 to 1.0 Ma. Changes in SST

distributions during the Pleistocene are important because they are considered to be linked to the mid-Pleistocene transition[50]. Applying the biomarker-based proxies, the Kazusa Group can provide a long, continuous, and high time-resolution palaeotemperature record in the Kuroshio region, which is integral to understanding Pleistocene climate changes.

Methods

Biomarker and organic compound analysis. Samples for biomarker analysis were freeze-dried after the surface was ultrasonically cleaned with ethanol and ground into fine powders. The lipids contained in the powdered sediment (~3 g) of each sample were extracted by sonication with dichloromethane/methanol (70:30, v/v) and then saponified with 0.5 mol L⁻¹ KOH in MeOH. The saponified sample was then extracted with _n_-hexane to obtain the neutral components. The neutral lipids were separated into four subfractions by silica gel column chromatography. The N-1 fraction (hydrocarbons) was extracted with _n_-hexane/dichloromethane (95:5, v/v), and the N-2 fraction (ketones, esters and aldehydes) with _n_-hexane/dichloromethane (4:6, v/v). Then, they were introduced into a gas chromatograph with a mass-selective detector (GC-MS) and a flame ionisation detector (GC-FID) equipped with a VF-5ms fused silica capillary column (30 m × 0.25 mm internal diameter, Agilent). The oven temperature was programmed as follows: maintained at 40 °C for 2 min, raised to 120 °C at 30 °C min⁻¹, raised to 300 °C at 6 °C min⁻¹, and maintained at 300 °C for 20 min. Several procedural blanks were analysed in parallel, under the same analysis conditions, and they showed no contamination. Analytical precisions (1σ) for $U^{K'}_{37}$, ACL and CPI were 0.002, 0.008 and 0.004 units, respectively. The powdered samples used for biomarker analysis were also used for total organic carbon (TOC) and total nitrogen (TN) analysis using a Flash 2000 CHNS elemental analyser. A powdered sample (~30 mg) was placed in a silver sample boat and decalcified with a few drops of 1 N HCl and then dried for at least 2 h at 80 °C to remove unreacted HCl and water. The dried samples were wrapped in a tin sample boat for combustion. Quantification errors for TOC and TN were both 3% (1σ) based on replicated analyses of a 2,5-bis-(5-tertbutyl-benzoxazol-2-yl)-thiophene standard. In this study, C/N ratios were used to clarify the source of organic matter, as the C/N ratio of typical marine phytoplankton organic matter is 6–7, whereas that of terrestrial organic matter is >12 due to the contribution of lignin-phenols[52].

Mg/Ca ratio analysis. Mg/Ca ratios of the planktic foraminifera _G. bulloides_ were analysed for five selected siltstone beds with relatively large amounts of foraminiferal standing stock and good preservation to reproduce the surface temperature. Samples for handpicking fossil foraminifera were disaggregated using Na₂SO₄. Mg/Ca ratios were measured using _G. bulloides_ from the >210 μm size fraction. Ten or more white-coloured clean individuals, without any dark-coloured surface (supposed to be an oxide film), were used for the measurements. The samples were cleaned using the following methods outlined by Cheng et al.[53]. We modified the methods for the foraminiferal tests following Yoshimura et al.[54]. Initially, the samples were gently crushed into fragments and then rinsed with methanol and ultrapure water. This process was repeated until all the loose material (i.e., nannofossils and clay) was removed. The samples were then treated with an oxidising agent that consisted of H₂O₂ and KOH to remove organic matter. Finally, the samples were rinsed with a mixture of H₂O₂ and HClO₄. Mg, Ca and Mn concentrations were obtained by inductively coupled plasma mass spectrometry (ICP-MS). For ICP-MS analysis, a powdered carbonate sample was transferred to Teflon vials, and 0.3 M HNO₃ was added to each vial to dissolve the solids. The HNO₃ used in this study was a commercially supplied high-purity TAMAPURE AA-100 reagent (Tama Chemical, Japan). To control the instrumental drift, internal standards (Be, Sc, Y and I) were added to HNO₃. In addition, standard solutions prepared from JCp-1 (Geological Survey of Japan)[55] were measured for use in data correction. The relative standard deviation based on replicate measurements of JCp-1 was 0.5% (1σ). The Mn/Ca ratios were 0.5 mmol

mol^{-1} or less for all measured samples, indicating that the precleaning was sufficiently performed[56]. The Mg/Ca ratios of *G. bulloides* were converted to a temperature scale using the calibration given by Mashiotta and co-workers[57].

Data availability

All data can be found in the Supplementary Materials as well as the database provided by NOAA National Centres for Environmental Information (NECI). URL: https://www.ncdc.noaa.gov/paleo-search/study/32152.

References

1. Marlowe, I. T. et al. Long chain (*n*-C$_{37}$–C$_{39}$) alkenones in the Prymnesiophyceae. Distribution of alkenones and other lipids and their taxonomic significance. *Br. Phycol. J.* **19**, 203–216 (1984).
2. Prahl, F. G., Muehlhausen, L. A. & Zahnle, D. L. Further evaluation of long-chain alkenones as indicators of paleoceanographic conditions. *Geochim. Cosmochim. Acta* **52**, 2303–2310 (1988).
3. Müller, P. J., Kirst, G., Ruhland, G., Von Storch, I. & Rosell-Melé, A. Calibration of the alkenone paleotemperature index U$_{37}^{K'}$ based on core-tops from the eastern South Atlantic and the global ocean (60° N–60° S). *Geochim. Cosmochim. Acta* **62**, 1757–1772 (1998).
4. Conte, M. H., Thompson, A., Lesley, D. & Harris, R. P. Genetic and physiological influences on the alkenone/alkenoate versus growth temperature relationship in *Emiliania huxleyi* and *Gephyrocapsa oceanica*. *Geochim. Cosmochim. Acta* **62**, 51–68 (1998).
5. Eglinton, G. & Hamilton, R. J. in *Chemical Plant Taxonomy* (Elsevier B.V., 1963).
6. Rielley, G., Collier, R. J., Jones, D. M. & Eglinton, G. The biogeochemistry of Ellesmere Lake, UK–I: source correlation of leaf wax inputs to the sedimentary lipid record. *Org. Geochem.* **17**, 901–912 (1991).
7. Baczynski, A. A., McInerney, F. A., Freeman, K. H. & Wing, S. L., Bighorn Basin Coring Project (BBCP) Science Team. Carbon isotope record of trace *n*-alkanes in a continental PETM section recovered by the Bighorn Basin Coring Project (BBCP). *Paleoceanogr. Paleoclimatol.* **34**, 853–865 (2019).
8. Sawada, K., Ono, M., Nakamura, H. & Tareq, S. M. Reconstruction of Holocene Optimum paleoclimatic variations using long-chain n-alkanes and alkenones in sediments from Dabusu Lake, northeastern China. *Quat. Int.* **550**, 27–38 (2020).
9. Rabinowitz, H. S., Polissar, P. J. & Savage, H. M. Reaction kinetics of alkenone and n-alkane thermal alteration at seismic timescales. *Geochemistry, Geophys. Geosystems* **18**, 204–219 (2017).
10. Wang, C., Eley, Y., Oakes, A. & Hren, M. Hydrogen isotope and molecular alteration of n-alkanes during heating in open and closed systems. *Org. Geochem.* **112**, 47–58 (2017).
11. Cleaveland, L. C. & Herbert, T. D. Preservation of the alkenone paleotemperature proxy in uplifted marine sequences: a test from the Vrica outcrop, Crotone, Italy. *Geology* **37**, 179–182 (2009).
12. Herbert, T. D., Ng, G. & Peterson, L. C. Evolution of Mediterranean sea surface temperatures 3.5–1.5 Ma: regional and hemispheric influences. *Earth Planet. Sci. Lett.* **409**, 307–318 (2015).
13. Ito, M. & Katsura, Y. Inferred glacio-eustatic control for high-frequency depositional sequences of the Plio-Pleistocene Kazusa Group, a forearc basin fill in Boso Peninsula, Japan. *Sediment. Geol.* **80**, 67–75 (1992).
14. Kazaoka, O. et al. Stratigraphy of the Kazusa Group, Boso Peninsula: an expanded and highly-resolved marine sedimentary record from the Lower and Middle Pleistocene of central Japan. *Quat. Int.* **383**, 116–135 (2015).
15. Okada, M., Suganuma, Y., Haneda, Y. & Kazaoka, O. Paleomagnetic direction and paleointensity variations during the Matuyama–Brunhes polarity transition from a marine succession in the Chiba composite section of the Boso Peninsula, central Japan. *Earth Planets Space* **69**, 45 (2017).
16. Suganuma, Y. et al. Paleoclimatic and paleoceanographic records through Marine Isotope Stage 19 at the Chiba composite section, central Japan: a key reference for the Early–Middle Pleistocene Subseries boundary. *Quat. Sci. Rev.* **191**, 406–430 (2018).
17. Haneda, Y., Okada, M., Kubota, Y. & Suganuma, Y. Corrigendum to "Millennial-scale hydrographic changes in the northwestern Pacific during marine isotope stage 19: teleconnections with ice melt in the North Atlantic". *Earth Planet. Sci. Lett.* **534**, 116107 (2020).
18. Haneda, Y., Okada, M., Suganuma, Y. & Kitamura, T. A full sequence of the Matuyama–Brunhes geomagnetic reversal in the Chiba composite section, Central Japan. *Prog. Earth Planet Sci.* **7**, 44 (2020).
19. Kameo, K., Kubota, Y., Haneda, Y., Suganuma, Y. & Okada, M. Calcareous nannofossil biostratigraphy of the Lower–Middle Pleistocene boundary of the GSSP, Chiba composite section in the Kokumoto Formation, Kazusa Group, central Japan, and implications for sea-surface environmental changes. *Prog. Earth Planet Sci.* **7**, 36 (2020).
20. Suganuma, Y. et al. Formal ratification of the Global Boundary Stratotype Section and Point (GSSP) for the Chibanian Stage and Middle Pleistocene Subseries of the Quaternary System: the Chiba Section, Japan. *Episodes J. Int. Geosci.*, https://doi.org/10.18814/epiiugs/2020/020080 (2021).
21. Kida, S. et al. in *"Hot Spots" in the Climate System* (Springer, 2016).
22. Tada, R., Zheng, H. & Clift, P. D. Evolution and variability of the Asian monsoon and its potential linkage with uplift of the Himalaya and Tibetan Plateau. *Prog. Earth Planet. Sci.* **3**, 4 (2016).
23. Hirayama, J. & Nakajima, T. Analytical study of turbidites, Otadai Formation, Boso Peninsula, Japan. *Sedimentology* **24**, 747–779 (1977).
24. Tsuji, T. et al. High-resolution chronology of the lower Pleistocene Otadai and Umegase Formations of the Kazusa Group, Boso Peninsula, central Japan—Chronostratigraphy of the JNOC TR-3 cores based on oxygen isotope, magnetostratigraphy and calcareous nannofossil. *J. Geol. Soc. Japan* **111**, 1–20 (2005).
25. Oyama, T., Chigira, M., Ohmura, N., Sasaki, K. & Nagaoka, T. Chemical weathering of sedimentary rocks in Vadose Zone – The weathering rates of mudstone on old unlined tunnel walls and the bacterial effects on it. *Japan Soc. Eng. Geol.* **39**, 511–523 (1999).
26. Nanayama, F., Nakazato, H., Ooi, S. & Nakashima, R. *Geology of the Mobara District. Quadrangle Series, 1:50,000* (Geological Survey of Japan, AIST, 2016).
27. Utsunomiya, M. & Ooi, S. *Geology of the Kazusa-Ohara District. Quadrangle Series, 1:50,000* (Geological Survey of Japan, AIST, 2019).
28. Kamiya, N. et al. Major variations in vitrinite reflectance and consolidation characteristics within a post-middle Miocene forearc basin: a geodynamical implication for basin evolution. *Tectonophysics* **710**, 69–80 (2017).
29. Prahl, F. G., De Lange, G. J., Lyle, M. & Sparrow, M. A. Post-depositional stability of long-chain alkenones under contrasting redox conditions. *Nature* **341**, 434–437 (1989).
30. Sawada, K., Handa, N. & Nakatsuka, T. Production and transport of long-chain alkenones and alkyl alkenoates in a sea water column in the northwestern Pacific off central Japan. *Mar. Chem.* **59**, 219–234 (1998).
31. Ohkouchi, N., Kawamura, K., Kawahata, H. & Taira, A. Latitudinal distributions of terrestrial biomarkers in the sediments from the Central Pacific. *Geochim. Cosmochim. Acta* **61**, 1911–1918 (1997).
32. Bendle, J., Kawamura, K., Yamazaki, K. & Niwai, T. Latitudinal distribution of terrestrial lipid biomarkers and n-alkane compound-specific stable carbon isotope ratios in the atmosphere over the western Pacific and Southern Ocean. *Geochim. Cosmochim. Acta* **71**, 5934–5955 (2007).
33. Rao, Z. et al. Compound specific δD values of long chain n-alkanes derived from terrestrial higher plants are indicative of the δD of meteoric waters: evidence from surface soils in eastern China. *Org. Geochem.* **40**, 922–930 (2009).
34. Luo, P., Peng, P., Lü, H., Zheng, Z. & Wang, X. Latitudinal variations of CPI values of long-chain n-alkanes in surface soils: evidence for CPI as a proxy of aridity. *Sci. China Earth Sci.* **55**, 1134–1146 (2012).
35. Zhang, J., Yu, H., Jia, G., Chen, F. & Liu, Z. Terrestrial n-alkane signatures in the middle Okinawa Trough during the post-glacial transgression: control by sea level and paleovegetation confounded by offshore transport. *Geo-Mar. Lett.* **30**, 143–150 (2010).
36. Müller, P. J., Čepek, M., Ruhland, G. & Schneider, R. R. Alkenone and coccolithophorid species changes in late Quaternary sediments from the Walvis Ridge: Implications for the alkenone paleotemperature method. *Palaeogeogr. Palaeoclimatol. Palaeoecol.* **135**, 71–96 (1997).
37. McClymont, E. L., Rosell-Melé, A., Giraudeau, J., Pierre, C. & Lloyd, J. M. Alkenone and coccolith records of the mid-Pleistocene in the south-east Atlantic: implications for the U$_{37}^{K'}$ index and South African climate. *Quat. Sci. Rev.* **24**, 1559–1572 (2005).
38. Yamamoto, M., Oba, T., Shimamune, J. & Ueshima, T. Orbital-scale anti-phase variation of sea surface temperature in mid-latitude North Pacific margins during the last 145,000 years. *Geophys. Res. Lett.* **31**, L16311 (2004).
39. Lisiecki, L. E. & Raymo, M. E. A Pliocene-Pleistocene stack of 57 globally distributed benthic δ^{18}O records. *Paleoceanography* **20**, PA1003 (2005).
40. Elderfield, H. et al. Evolution of ocean temperature and ice volume through the mid-Pleistocene climate transition. *Science* **337**, 704–709 (2012).
41. Nürnberg, D., Bijma, J. & Hemleben, C. Assessing the reliability of magnesium in foraminiferal calcite as a proxy for water mass temperatures. *Geochim. Cosmochim. Acta* **60**, 803–814 (1996).
42. Kuroyanagi, A. & Kawahata, H. Vertical distribution of living planktonic foraminifera in the seas around Japan. *Mar. Micropaleontol.* **53**, 173–196 (2004).
43. Oba, T. & Murayama, M. Sea-surface temperature and salinity changes in the northwest Pacific since the Last Glacial Maximum. *J. Quat. Sci.* **19**, 335–346 (2004).

44. Oda, M. & Yamasaki, M. Sediment trap results from the Japan Trench in the Kuroshio domain: seasonal variations in the planktic foraminiferal flux. *J. Foraminiferal Res.* **35**, 315–326 (2005).

45. Nürnberg, D., Müller, A. & Schneider, R. R. Paleo-sea surface temperature calculations in the equatorial east Atlantic from Mg/Ca ratios in planktic foraminifera: a comparison to sea surface temperature estimates from $U_{37}^{K'}$, oxygen isotopes, and foraminiferal transfer function. *Paleoceanography* **15**, 124–134 (2000).

46. Bard, E. Comparison of alkenone estimates with other paleotemperature proxies. *Geochemistry, Geophys. Geosystems* **2**, https://doi.org/10.1029/2000GC000050 (2001).

47. Kuroyanagi, A., Kawahata, H., Nishi, H. & Honda, M. C. Seasonal to interannual changes in planktonic foraminiferal assemblages in the northwestern North Pacific: sediment trap results encompassing a warm period related to El Niño. *Palaeogeogr. Palaeoclimatol. Palaeoecol.* **262**, 107–127 (2008).

48. Sawada, K. & Handa, N. Variability of the path of the Kuroshio ocean current over the past 25,000 years. *Nature* **392**, 592–595 (1998).

49. Oba, T. & Yasuda, H. Paleoenvironmental change of the Kuroshio region since the last glacial age. *The Quat. Res.* **31**, 329–339 (1992).

50. McClymont, E. L., Sosdian, S. M., Rosell-Melé, A. & Rosenthal, Y. Pleistocene sea-surface temperature evolution: early cooling, delayed glacial intensification, and implications for the mid-Pleistocene climate transition. *Earth Sci. Rev.* **123**, 173–193 (2013).

51. Fedorov, A. V., Burls, N. J., Lawrence, K. T. & Peterson, L. C. Tightly linked zonal and meridional sea surface temperature gradients over the past five million years. *Nat. Geosci.* **8**, 975–980 (2015).

52. Lamb, A. L., Vane, C. H., Wilson, G. P., Rees, J. G. & Moss-Hayes, V. L. Assessing $\delta^{13}C$ and C/N ratios from organic material in archived cores as Holocene sea level and palaeoenvironmental indicators in the Humber Estuary, UK. *Mar. Geol.* **244**, 109–128 (2007).

53. Cheng, H., Adkins, J., Edwards, R. L. & Boyle, E. A. U-Th dating of deep-sea corals. *Geochim. Cosmochim. Acta* **64**, 2401–2416 (2000).

54. Yoshimura, T. et al. Altervalent substitution of sodium for calcium in biogenic calcite and aragonite. *Geochim. Cosmochim. Acta* **202**, 21–38 (2017).

55. Okai, T. Collaborative analysis of GSJ/AIST geochemical reference materials JCp-1 (Coral) and JCt-1 (Giant Clam). *Geochemistry* **38**, 281–286 (2004).

56. Hasenfratz, A. P. et al. Determination of the Mg/Mn ratio in foraminiferal coatings: an approach to correct Mg/Ca temperatures for Mn-rich contaminant phases. *Earth Planet. Sci. Lett.* **457**, 335–347 (2017).

57. Mashiotta, T. A., Lea, D. W. & Spero, H. J. Glacial–interglacial changes in Subantarctic sea surface temperature and $\delta^{18}O$-water using foraminiferal Mg. *Earth Planet. Sci. Lett.* **170**, 417–432 (1999).

58. Wessel, P. & Smith, W. H. F. New, improved version of Generic Mapping Tools released. *EOS Trans. Am. Geophys. Union* **79**, 579 (1998).

59. Utsunomiya, M., Mizuno, K., Naya, T., Omura, K. & Nagai, M. Correlation between a Tephra Bed from Deep (2038 m) Underground below Chiba City, and Kd48 in the Lowermost Kiwada Formation (Lower Pleistocene). *J. Geogr. (Chigaku Zasshi)* **129**, 355–374 (2020).

Author contributions

H. Kajita and M.U. designed the project and conducted the field survey. H. Kajita and A.M. analysed the samples. T.Y., N.O., A.S. and H. Kawahata organized the laboratory work and contributed toward data interpretation. H. Kajita wrote the manuscript. All authors contributed toward editing and revising the manuscript.

Competing interests

The authors declare no competing interests.

Additional information

Supplementary information The online version contains supplementary material available at https://doi.org/10.1038/s43247-021-00154-2.

Correspondence and requests for materials should be addressed to H.K.

Peer review information Primary handling editors: Rachael Rhodes, Joe Aslin

Reprints and permission information is available at http://www.nature.com/reprints

Publisher's note Springer Nature remains neutral with regard to jurisdictional claims in published maps and institutional affiliations.